ARMA 13-584

Multi-scale fracture creation and network generation during fracturing

Johnson, S.
Lawrence Livermore National Laboratory, Livermore, California, USA
Arson, C.
Georgia Institute of Technology, Atlanta, Georgia, USA
Settgast, R.
Lawrence Livermore National Laboratory, Livermore, California, USA

ABSTRACT: Here we describe both a sequential, hierarchical multi-scale approach for designing scale-dependent constitutive models at different levels of refinement in the problem as well as an open-source, massively parallel software platform (GEOS) used for implementing the approach. General cross-scale coupling is achieved through a variety of terms, which are tailored to the specific physical mechanisms involved. The focus in this paper is on the specific state of fracture and damage propagation under fluid forcing, including seismic source generation, directionality and criteria for nucleation and growth, especially in the presence of multi-scale discontinuities. To address computational complexity issues, we discuss strategies for handling under-resolution at the crack tip and the design of phenomenological models based on finer scale considerations in two dimensions. We also discuss progress on approaching the three dimensional case as well as preliminary results of simulations to predict the evolution of micro-seismicity resultant from progressive damage under changing subsurface stress and hydrological conditions.

1. INTRODUCTION

"Multi-scale simulation" has become an oft-used term in numerical modeling, but its utility in addressing problems of practical interest has been elusive within the jointed rock mechanics and unconventional reservoir simulation communities. The reasons behind this are manifold, but the main issues are the vast separation of scales involved (at least $O(10^{-4})$ *m* to $O(10^{3})$ *m*) combined with the lack of strict scale-independent similarity, the paucity and/or large uncertainty bounds of data at different scales as well as its interpretation, and the absence of a theoretical framework to link data gathered at finer scales to the phenomenology observed at coarser scales. This paper focuses on addressing the last point and focusing on the problem of hydraulic fracture propagation in the subsurface.

Hydraulic fracture stimulation has been in use since at least the 1860's when the first United States patents on "torpedoing" were issued for use of explosive charges in stimulating water wells in the eastern U.S. [1]. The use of hydraulic fracturing for stimulating a shale gas reservoir was first performed experimentally at Kelpper Well No. 1 in the Hugoton field of Kansas [2]. Though a useful strategy for stimulating reservoirs, especially compared with acidizing treatments, the coupling with horizontal dilling and "slickwater" (i.e., water with friction-reduction agents) as the working fluid has created a technological breakthrough and the exponentially increasing commercial development of large volumes of natural gas deposits in tight formations since the late 1990's [3]. This spike in production has influenced world gas prices, which are currently significantly depressed in the US; however, the same technology used to spur the growth of shale gas is also leading to significant increases in the development of shale oil and co-produced oil (with gas). Despite the expansion of this industry, there is still the opportunity for significant increases in efficiency; for instance, the NETL estimates that of the 1500 tcf original gas in place (OGIP), only 262 tcf (17%) is technically recoverable [4].

Part of the reason it is difficult to increase rates of recovery is that there remains a need to improve understanding and prediction of the behavior of the reservoir with respect to stimulation. This may include not only improved measurements but also improved interpretation of measurements. Currently, micro seismic monitoring is one of the few commercially proven ways to acquire data on the stimulation process. Though data analysis for the location, mechanism, and magnitude of microseisms has improved, the constraint on the interpretation of this data remains coarse, and it is still an open question what these sources mean both in terms

of fracture network evolution and its impact on short- and long-term permeability and production. For instance, Moos [5] reported that for the same well with two similarly performing stages, the observed micro seismicity can be drastically different between the two. It is also an open question as to whether and to what extent aseismic failure events, which cannot be detected through micro seismic analysis, occur in a stimulated reservoir, as investigated by Zoback [6]. Both the interpretation of the meaning of the microseismic data and the inference of aseismic events require a model, either analytical or numerical.

The current state of such models at the commercial level is significantly computationally constrained by the requirements that models run within minutes on a standard desktop, so much of the development of such tools has focused on empirically derived functions and low-fidelity but highly efficient numerical techniques to achieve the greatest possible fidelity for a modest computational cost. For instance, to capture fracture propagation many rely on models predicated on the assumptions of the Perkins-Kern-Nordgren (PKN) model [7] of quasi-3D fracture propagation in a linearly elastic, isotropic medium, which is a set of assumptions easily violated in most anisotropic, bedded lithologies of interest in shale gas reservoirs.

This type of approach has largely restricted such tools to calibration based on current technology and is naturally sensitive to the assumptions of the model. If we want to achieve further improvements in understanding these fractured unconventional reservoirs and if we want to better predict the outcomes for untried stimulation techniques or stimulation techniques without a significant history, we will likely need to redesign the modeling methodology to include targeted upscaling of fine scale phenomenology to coarse scales, at which we can perform computationally tractable simulations. This paper will investigate this approach by first discussing the failure mechanisms that need to be captured and then how to capture these mechanisms numerically.

2. FAILURE MECHANISMS IN HYDRAULIC FRACTURING

For the case of a propagating fracture due to hydraulic fracture stimulation, micro-seismic data collected from a number of projects indicate bulk fracture propagation of $O(10^1)m/s << O(10^3)m/s$ for the Rayleigh wave speed in most geologic materials. This is counter-intuitive when considering fracture mechanics, where fractures in tension (Mode I) generally propagate near the Rayleigh wave speed. This remains true at the micro-scale; however, fracture propagation is constantly mediated by fluid forcing, which is dependent on maintaining a pressure front near the tip of the fracture. The time constant associated with this pressure front development is much larger than that associated with the Rayleigh wave speed. If we resort to theoretical consideration of fluid-driven fractures in an elastic medium, the anecdotally observed propagation velocity noted above is recovered [8]:

$$\lambda = 4\mu K^2 v \sigma_0^{-3} \qquad (1)$$

where μ is the viscosity, v is the mean fluid velocity into the fracture, K is the modulus of the fluid, and σ_0 is the confining pressure. For typical rock properties at confining pressures of 10-100 MPa, the tip velocity is *O(1-10) m/s*.

In general, this suggests stress equilibrium in the far field for bulk fracture propagation, such that there exists a temporal scale separation between the resolution of stress in the local region of a fracture and that at larger scales. This region, referred to in the literature as the "process zone", can often be decoupled from the solution of the mechanics in the rest of the domain (referred to as the "far field"). For instance, numerical, multi-scale research [9-11] has suggested that scale-separation, when implemented in numerical models in practice, can predict crack fronts in mixed mode fracture situations where the forcing term is constant. For the case of a hydraulically-induced fracture, where fluid forcing controls the crack front propagation, the time constant is separated by an even greater scale, suggesting that this may be a viable path to multi-scale coupling. In addition, a number of experimental studies in brittle, homogeneous polymers are available for validation (e.g., [12]) of such multi-scale approaches.

Failure, however, in a realistic geological material can be much more complex than the isotropic, homogeneous, elasto-brittle materials classically addressed in the linear elastic fracture mechanics (LEFM) literature, especially given the bedded, anisotropic, and discontinuous nature of geologic material [13-17]. When focusing only on the mechanisms involved at the process zone of a propagating hydraulic fracture, the complexities of crack coalescence, fluid interaction, complex stress field anisotropy, and grain boundary effects can be readily seen, but complexities exist across length scales. Careful field studies and analyses [18] have, for instance, observed that discontinuities exhibit a smooth length scale distribution across scales from millimeters to kilometers and are widely believed to be due to growth processes that do not have characteristic length scales [19-20].

In this study, we focus on how to resolve this problematic situation via a sequential, hierarchical multi-scale method, which, at its base, relies on a dual-scale representation of inhomogeneity and damage. By

overlapping the spatial scales at which successively coarser simulations are performed, effective upscaling can be managed and scale-dependent relations with appropriate contributions from finer scales can be developed. In order to provide a link between the scales for the propagation of a fracture, we appeal to strain-parameterized phenomenological models, which have been previously described by Fu [21-22], to resolve coarser scales, and we rely on a cohesive zone method [23] to directly calculate fracture propagation at the finest scales. Topological changes in the mesh are resolved using a procedure similar to that detailed by Settgast [24]. For failures along pre-existing surfaces, we use a numerical framework similar to that described in Vorobiev [25] but amended to accommodate arbitrarily large strains through an advection-free scheme; the amendments are described next for completeness, as they have not been previously described in the literature.

3. FAILURE ALONG INTERFACES

For the case of failures either along the developed fracture network or in regions where the stress field has been rotated enough to effect failure in pre-existing fractures, the failures are often Mode II (strike-slip) events, as they are predominantly for laboratory hydraulic fracture experiments [26-28]. A number of joint constitutive models can capture this effect as well as other salient features of the hydro-mechanical joint response [29-37]. There have been a number of studies that have helped to elucidate the functional relationship between fracture permeability and roughness, shear, normal stress, and other parameters, which are too numerous to list here. In addition to pure shear behavior, many of these models capture both dilatant behavior as well as compaction.

Because we are focusing on the evolution of micro seismicity here, we focus on a particular joint mechanics model, Ruina-Dieterich [38-39], for resolving shear failure as a function of rate effects and other time-dependent mechanisms (so-called “rate-and-state” type friction model). However, the GEOS framework implements a number of joint constitutive models.

In order to appropriately evaluate these models within a numerical code, an appropriate method must first be developed.

3.1. Numerical Resolution of Failure Along Interfaces

One problem that has yet to be addressed is the ability to capture arbitrarily large shear strains at the interfaces of moving joints in a tractable numerical framework, where the behavior at the interface is represented by phenomenological joint models. We address this through an advection-free scheme based on the common plane method often used in the discrete element method (DEM). One example of using such a method in a finite difference code is detailed in Vorobiev [25]; however, such a scheme degrades under significant strain at the interface, as demonstrated in Fig. 1 and also exhibits other pathological behaviors due to its failure to ensure conservation of momentum. Fig. 1 also illustrates how the previous algorithm masks a potentially difficult to diagnose pathology in shear, since shear strain energy is gained (due to recognition of new elastically-deforming surfaces) at approximately the same rate it is lost to numerical advection, which may be erroneously interpreted as a frictional effect.

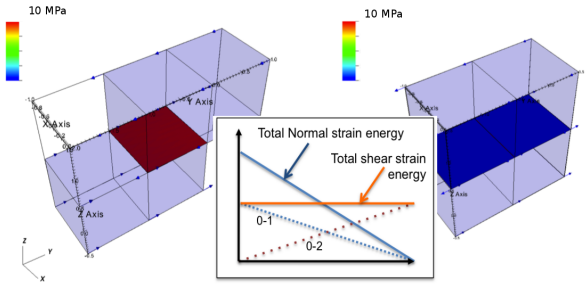

Fig. 1. Description of simple numerical demonstration of Vorobiev [25] where elements are brought into contact normally, then sheared; the color bars indicate elastic strain energy at the interface (blue is 0 MPa), where shearing causes normal strain energy loss due to numerical advection. The dotted lines indicate the energy associated with face pairs (face index 0 is the face associated with the top mesh and face indices 1 and 2 are associated with the bottom faces, where 0-1 is the initial face pair in contact).

To remove the advection dependence, we use an independent contact element associated with a pair of external mesh faces. The state variables associated with the contact element are then homogenized as composite state variables associated with the external mesh faces. When a new contact element is created, it inherits the homogenized state from the area-weighted contributions of the states associated with the constituent faces, as detailed in the following discussion. By using an essentially Lagrangian technique to track the contact evolution and using a remapping technique to spawn new contacts, the method avoids advection-related numerical issues.

The states associated with the external faces can be initialized in the same manner as those for the contact elements. When an external face is associated with a contact element, however, it uses an area-weighted homogenization scheme to cache the contact element's contribution to its state.

$$\tilde{A}_{i,k} = \begin{cases} A_k^{cel} & \text{where face "i" composes part of contact element "k"} \\ 0 & \text{otherwise} \end{cases} \quad (2)$$

where $\tilde{A}_{i,k}$ is the area of face i composing part of contact area k.

$$f_i^n = \sum_{k=0}^{k<n_{cel}} \frac{\tilde{A}_{i,k}}{\hat{A}_i} \tilde{f}_k^n \tag{3}$$

where n_{cel} is the number of contact elements, $\hat{A}_i$ is the area of face i that intersects the region of any contact element, $\tilde{f}_k^n$ is the n^{th} state associated with contact element k, and f_i^n is the n^{th} state associated with face i. When a new contact element is spawned as the result of an external face pair coming into geometric intersection, the contact initializes its state from the area-weighted states of its constituent external faces:

$$\tilde{f}_k^n = \sum_{i=0}^{i<2} \frac{A_{i,k}}{\sum_{j=0}^{j<2} A_j} f_i^n \tag{4}$$

where $A_{i,k}$ is the area of the i^{th} face locally indexed to contact element k.

The result of this procedure is an advection-free method of representing large strains across interfaces. This can be illustrated in the same example as Fig. 1, using the new advection-free algorithm (Fig. 2).

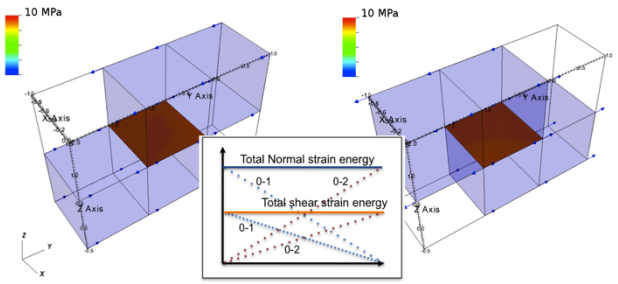

Fig. 2. Simple numerical demonstration of improved, advection-free contact approach for arbitrarily large shear strain, where elements are brought into contact normally, then sheared while conserving energy. The color bars indicate elastic strain energy at the interface (blue is 0 MPa). The dotted lines indicate the energy associated with face pairs (face index 0 is the face associated with the top mesh and face indices 1 and 2 are associated with the bottom, where 0-1 is the initial face pair in contact).

Separately, the algorithm also assures linear and angular momentum conservation by evaluating the shape function derivatives of the finite elements on the external faces and applying the resultant forces from the phenomenological joint models to the nodes, accordingly.

With the development of the appropriate numerical infrastructure to assess failure along joints in this section as well as appropriate treatment of the fracture nucleation and propagation at both fine and coarse scales alluded to in the previous section, the numerical method is complete with respect to the necessary components to enable a sequential, hierarchical multi-scale approach. What remains to complete the description of the method is the details of the particular dual-scale representations as well as the coupling terms to be used to bridge the scales. These will be described next.

4. THERMODYNAMIC, MATHEMATICAL, AND NUMERICAL CHALLENGES OF BRIDGING SCALES

From the previous discussion, it is clear that geomaterials exhibit two main attributes that make them natural candidates for a multi-scale treatment: the phenomenology of interest possesses no similarity relations across scales and the size distribution of discontinuities is smooth across several orders of magnitude, making it impossible to rigorously define a representative volume element (RVE) for the general case (though, specific systems may exhibit natural scale decoupling). The former means that models will likely need to be scale-dependent, while the latter means that material behavior cannot be characterized locally and, therefore, effective continuum representations will always have some error associated with the locality assumption. The situation is not hopeless, though. There are many field cases where the assumptions of an effective continuum do hold or at least do not introduce significant error; analysts can often identify natural scale decoupling due to the specific geology (e.g., local features limit the size distribution of the discontinuities), or the phenomenology of interest is not affected by the discontinuities (e.g., long period wave propagation). We are concerned with the cases where the system does not permit such simplifications and which require consideration of many scales.

4.1. The Dual Scale Paradigm

We develop our approach to multi-scale modeling through the assumption that for any arbitrary length scale, discontinuities can be represented at two scales, either the response of each discontinuity is represented directly (explicitly) and material response is defined through the aggregate of individual discontinuities (i.e., discontinuous modeling) or through homogenization of the behavior of a RVE of such features (i.e., effective continuum). The approach in GEOS seeks to represent both scales at any particular arbitrary length scale, where discontinuities near the length scale of interest are represented explicitly while features smaller than a threshold are represented via an effective continuum, where the constitutive model used is necessarily scale-dependent and derived from finer scale simulations when the scale of the RVE is above the percolation limit. This type of approach is illustrated in Fig. 3.

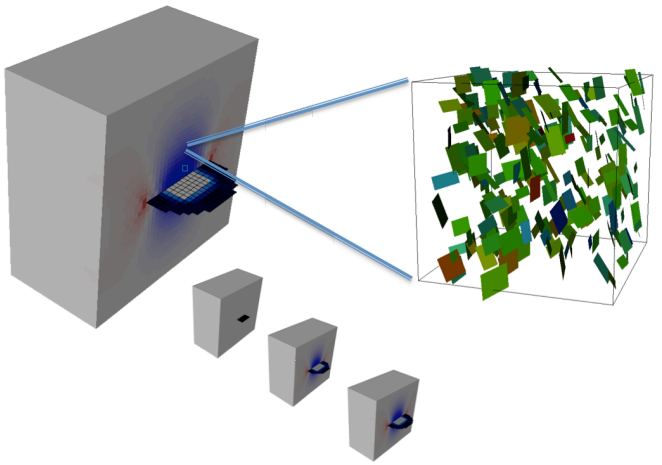

Fig. 3. Simple illustration of a propagating, penny-shaped hydraulic fracture, where the RVE-scale response is characterized by a scale-dependent constitutive model derived from simulations at finer scales.

4.2. Explicit Representation of Fracture Nucleation and Propagation

Linear Elastic Fracture Mechanics (LEFM) allows the prediction of the propagation of a single, flat crack (or fracture) embedded in a homogeneous, isotropic, elastic solid body. The analytical solutions derive from Griffith theory and can be obtained by computing Stress Intensity Factors (SIFs) in modes I, II and III. As a consequence, most of the existing models of hydraulic fracturing consider the rock mass as an elastic, impermeable solid. This approach is suitable to distinguish between toughness-dominated and viscosity-dominated fracture propagation regimes [40], but it is constrained by restrictive assumptions and does not allow coupling fracture propagation to the fabric changes undergone by the rock mass. Neglecting micro-cracking ahead of the fracture tip leads to over-estimated fracture front velocity [41-42]. Moreover, according to the theory of elasticity, the presence of cracks around the fracture tip induces stress perturbations, and thus impact SIFs. Some work has been proposed to address this [22]; however, this remains an open research issue for fully three-dimensional solids. Crack arrays parallel to the fracture plane have a shielding effect, whereas crack arrays perpendicular to the fracture plane tend to favor fracture propagation [21, 43].

One method of capturing the damage zone in finite element models of hydraulic fracturing is to define an inelastic zone where plastic deformation localizes [44-5]. The numerical solution is highly mesh-dependent, however, and the localized zone narrows with mesh-refinement. For unstructured meshes, this leads to an asymmetric plastic zone even when the problem is symmetric relative to the fracture plane. Displacement-based methods, such as Fu [22], seek to address this issue.

4.3. Effective Continuum Representations

There are a number of approaches to represent the effective hydrological and mechanical response of geomaterials to progressive damage. These can be categorized into micro-scale derived models, purely phenomenological models, micro-scale enriched methods (with varying levels of fidelity), and hybrids of the aforementioned. There are also special considerations for calculating the effects on permeability through the use of homogenization techniques.

Here we are using a hybrid model of damage nucleation and accumulation at the effective continuum scale, where the micro-scale degrees-of-freedom are explicitly captured using finite, rectilinear failure surfaces, as illustrated in Fig. 3. We are currently using small damage assumptions, as well, where micro-scale damage does not evolve mechanical changes at the macro-scale. This is a strong assumption that will be remediated in further work.

5. THE GEOS SIMULATION FRAMEWORK

The previously described numerical approaches to explicitly capturing both fine and coarse scale fracture initiation and propagation as well as the effective continuum method for capturing the same at sub-RVE scales must be implemented within a numerical framework if the developments are to be applicable to problems of practical interest.

This framework, at a minimum, must include the appropriate facilities for:

- Large-scale (i.e., high performance computing) calculation and communication
- Appropriate solvers for the numerical approaches
- Facilities to provide dynamic topological changes in parallel for unstructured meshes
- Data structures optimized for the communication and calculation requirements
- Appropriate material modeling framework with the ability for users to easily add new models
- Massively parallel input and output

As part of a multi-year effort to address energy security issues in the geosciences, Lawrence Livermore National Laboratory has funded the Computational Geosciences group to design and implement the GEOS framework, which satisfies these requirements. Specifically, GEOS provides a general HPC simulation platform for Lagrangian computational geosciences applications with linear scaling at job sizes greater than 32 processes, as

illustrated in Fig. 4. Details are provided in previous works [67-9].

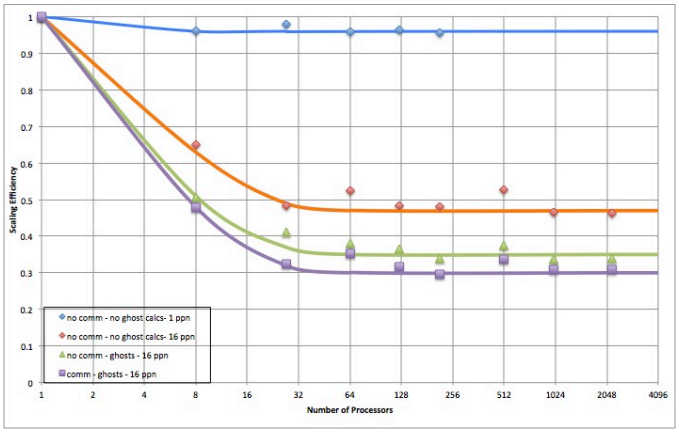

Fig. 4. Weak scaling study results for a simple, explicitly solved, hydromechanical (finite element / finite volume coupled) simulation in GEOS, where the coupling is similar to the described in Johnson [70]

Currently, a number of numerical techniques that leverage the massively parallel code infrastructure have been implemented within the GEOS framework, including finite element, finite volume, discrete element, and boundary element methods. Both implicit and explicit solvers are available, including a fully-coupled, implicit solver for hydromechanical problems with mesh topology changes, characteristic of hydraulic fracture stimulation problems. Though it is built to be a versatile platform, the specific focus of GEOS development is targeted at better characterizing reservoir response to fluid-induced perturbations, including different stimulation and fracture control techniques and enhanced geothermal systems (EGS). An example of this use case is illustrated in Fig. 5.

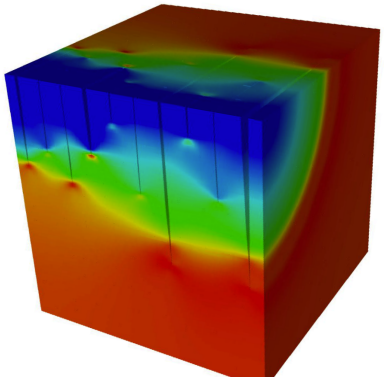

Fig. 5. Illustration of 3D quadrant of ten, propagating, penny-shaped hydraulic fractures in an elastic, homogeneous block courtesy of Dr. Pengcheng Fu. Color indicates stress in the axial direction (i.e., normal to the initial fracture plane) from blue to red (compressive to tensile). Slight perturbations in the pressure boundary conditions lead to "racing" conditions in the fracture propagation.

Besides hydraulic fracture stimulation and flow through fracture networks, the GEOS framework has also been applied to:

- Detailed hydro-chemo-mechanical (HCM) simulations of reactive flow and transport of CO2 through fractures [71].
- Evaluation of short- and long-term seismicity changes due to pore pressure perturbations along the fault (i.e., risk assessment for induced seismicity) based on the RSQSim approach of Dieterich and Richards-Dinger [72-5].

Care has been taken to make GEOS both developer friendly as well as standard compliant. For instance, GEOS is fully compliant with the C++11 standard and MPI v1.0, for distributed memory communication. It uses a fully validated XML input format as well as standard ABAQUS format mesh definitions. Parallel SILO (HDF5-based binary format) files are used for input of simulation restart states as well as for visualization and can easily be read an analyzed via the open source VisIt parallel visualization engine (see http://visit.llnl.gov).

6. CAPTURING MICROSEISMICITY

The problem of modeling micro seismicity is a particularly appropriate motivating problem for a multi-scale framework, as the phenomenology of interest is occurring at material scales that are below that directly representable with currently available HPC infrastructure. Many of the source mechanism in which we are interested are of the M_{-3} to M_0 magnitude ranges. For stress drops near 10 MPa and magnitude M_0 (the upper range of our consideration), the maximum slip is *O(1mm)* for an area of approximately 10 m^2, while the majority of events recorded in micro-seismic arrays are less than M_{-1}, as inspection of self-similarity relationships in frequency-magnitude would suggest, with associated slip of approximately the size of a sand grain, i.e., *O(200μm)*, and area of approximately 1 m^2 [76]. However, the inter-stage distance in many unconventional reservoirs is *O(100m)*. To accurately resolve even this part of the site at a scale where the faults generating the seismicity of interest can be resolved directly would require at a minimum *O(1e10)* elements, a computational expense approximately twice that of the world's current top supercomputer. Without the ability to directly capture the scales of interest, the question of how to leverage multi-scale techniques becomes one of practical necessity.

The issues that must be considered are manifold and include the ability to capture scale-dependent joint constitutive behavior, as described earlier, as well the

energy release as a function of time in the spectral range up to at least 25Hz, the maximum operating frequency of most arrays. The wave propagation resolution must also appropriately account for energy coupling between the source and matrix as well as the attenuation and spectral transformation (in the fully three-dimensional case) of the signal between the source and observation point(s). Ultimately, such capabilities can be used to statistically validate the model when used in conjunction with an uncertainty quantification framework. This generic workflow is illustrated in Fig. 6.

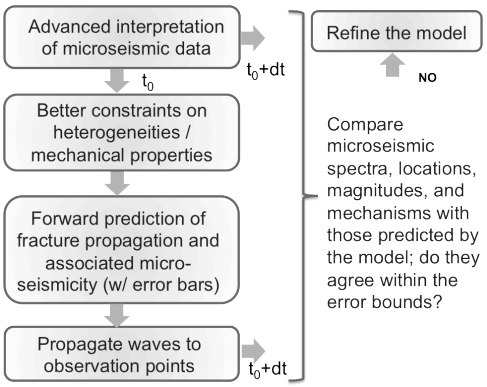

Fig. 6. Generic workflow for validation and calibration of GEOS via microseismic data

As we have adopted a microscale-derived continuum model approach for the multi-scale description of our materials, we need to have a method to quickly derive model behavior under a particular load path. That is, we need to run the model under a variety of load paths in order to derive the conjugate affinities and assess the model support described in Steps 1-3 of Section 4.3.1.

To determine whether the targeted approach could provide useful insight into the generation of micro seismicity, a simple defined strike slip scenario has been designed, which removes as much complexity from the approach as achievable with a goal of isolating the salient features of the sub-scale model necessary to capture the distribution of source mechanisms observed in practice. This model reduction makes the use of this approach computationally tractable.

Here, a geostatistically distributed set of sub-scale discontinuities were used to characterize the behavior at the sub-RVE scale while the homogeneous stress and strain states of the element (RVE scale) were used to inform the failure models at the sub-RVE scale. In this study, the discontinuities neither affect each other nor the stress state in the RVE, and the stress and strain states are uni-directionally coupled from the RVE scale. Progressive damage is also excluded in the model, and failure at the level of the discontinuity is instead represented by a simple shear-weakening law, which constrains the types of mechanisms that the model will represent. Fault orientations and spatial distribution are generated stochastically using a fault generator described in Johnson [70]. The relevant values for the distributions are as follows:

Table 1. Properties used in micro seismicity simulation

Property	**μ**	**σ**	**Min.**	**Max.**
τ_{fail}	10 kPa	3 kPa	1 kPa	100 kPa
δ_{strike}	30 cm	10 cm	1 mm	50 cm
δ_{dip}	20 cm	7 cm	1 mm	32 cm
θ_{strike}	90^o	9^o	56^o	132^o
θ_{dip}	70^o	15^o	45^o	90^o
fracture intensity	$16/m^3$	$6/m^3$	$0/m^3$	$30/m^3$

All discontinuities are rectilinear, and the top edge is parallel to the free surface. The values in Table 1 are the parameters for a Gaussian distribution of each property except the fracture intensity, which is fractally distributed with a Hurst exponent of 1.3. τ_{fail} is the shear stress at the onset of failure. δ_{strike} is the strike dimension. δ_{dip} is the dip dimension. θ_{strike} is the strike angle. θ_{dip} is the dip angle.

An RVE is populated by discontinuities sampled from the independent distributions described in Table 1 and then subject to a constant shear strain rate in simple strike-slip along strike angle 0^o. The simulation is run to a total shear strain of 0.008, and the cumulative seismic catalog at the end of the simulation was determined. The cumulative catalog at the end of the simulation is shown in Fig. 7 plotting the source mechanism tensor as represented by triaxial ellipsoids oriented in space where the size and color represent the total event magnitude associated with the discontinuity.

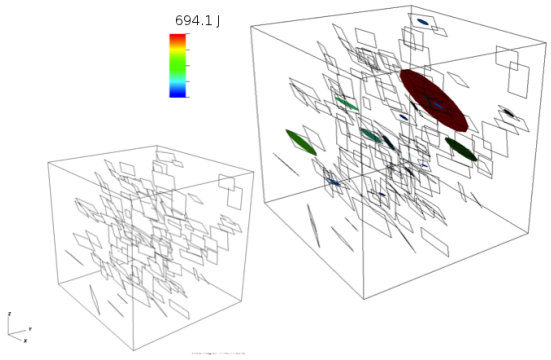

Fig. 7. Results of applied shear strain to an effective RVE of discontinuities, where the lower left figure shows the original realization of joints and the upper right plot shows the configuration overlaid with tensorial representations of all seismic events generated during the applied shear strain path. The color bar indicates increasing total energy release from blue to red, and the size, orientation, and relative size of the axes of the ellipsoids indicate the size and directionality of the synthesized moment tensors.

Plotting these results in a typical Hudson-type plot yields the representation in Fig. 8.

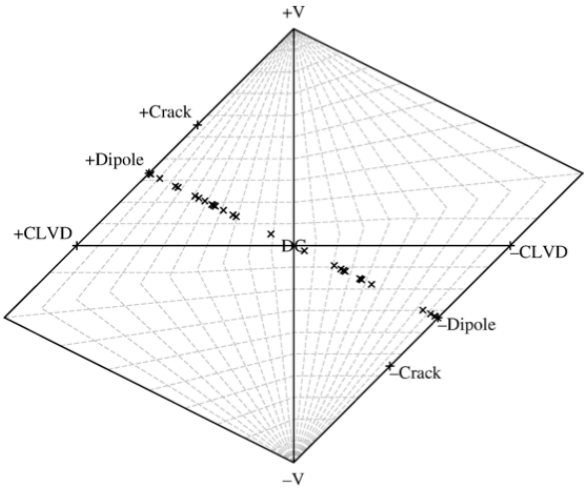

Fig. 8. Cumulative seismic source mechanism catalog plotted on a Hudson plot representation courtesy of Drs. Rob Mellors and Sean Ford.

Fig. 8 elucidates the imprinting of the source mechanism form enforced by the failure model; however, the simplification used not only captures the average trend often observed in field data, but it also captures the clustering of mechanisms near the +/- dipole intercepts and the relative sparsity of events near the double couple origin. This kind of result is encouraging, in that, it suggests an additive, rather than reductive, approach to the fidelity of model is possible for this problem. Interestingly, the most obvious drawback of the approach is the lack of spread away from the diagonal trend resultant from the strong imprinting of the source mechanism due to the simple failure mode. Including shear-induced dilation and compaction into the joint response via one of the currently implemented joint models in GEOS and using material properties appropriate to the geology of interest should provide the necessary richness to the joint response to capture the observed distribution.

7. RESULTS

For an initial study of the effects of fracture propagation on the generation of micro seismicity within the rock matrix, a pair of parallel stages are stimulated via fluid pressure boundary conditions at their intersection with the borehole and allowed to propagate.

The stress evolution in the direction of the horizontal borehole (x-axis) of the fractures is shown in Fig. 9. A slightly less dense fluid is pumped into the fracture at x=20m (1.11055 sg versus 1.11098 sg in the x=40m fracture), leading to asymmetries in the topology and extents of the final fractures. The compressive stress in the 20m interval between the two fractures, causes the initially parallel, planar fractures to curve away from each other during stimulation, leading to a characteristic "pie plate" geometry. The complex stress state also initiates fracture bifurcation in the x=40m fracture, as can be seen in Fig. 9 at the intercept with the y-axis at approximately -12m. The iso-contours (clipped at y=0m for clarity) show the double-lobed tensile stress annulus at the propagating fracture tips as well as the elevated x-direction compressive stresses that generally decrease with radial distance from the borehole.

By removing the stress iso-contours and adding micro seismic locations within the rock matrix, one can see the pattern of cumulative micro seismicity in Fig. 10. This micro seismicity is due to the rotation of the stress tensor due to the propagation of the hydraulic fractures. As the stress tensor rotates, that proportion of in situ joints that are preferentially oriented transition to failure and release a commensurate directional seismic energy as captured by the simple model discussed previously. The pattern of the micro seismicity tends to lead the fracture path.

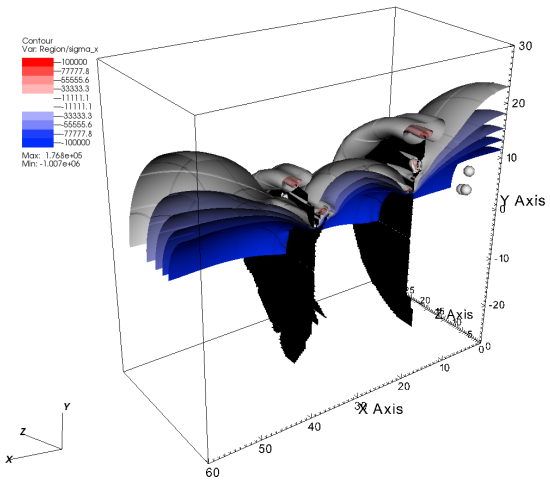

Fig. 9. Illustration of the final topology of two 3D, propagating, curved hydraulic fractures in an elastic, homogeneous rock matrix. The clipped quadrant iso-contours (upper quadrant) illustrate the stress in the x direction, clearly showing the resolved tensile stress along the propagating edge.

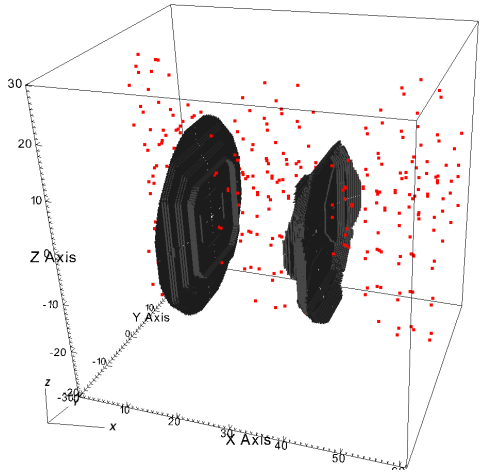

Fig. 10. Illustration as in Fig. 9 with the iso-contours removed for clarity and addition of cumulative micro seismic event locations within the rock matrix.

8. CONCLUSIONS

This study has demonstrated how the needs of the detailed modeling of hydraulic fracture propagation are complex both in terms of the needs for spatial and temporal multi-scale requirements. However, we have proposed a sequential, hierarchical multi-scale approach that leverages a dual-scale discontinuum/continuum representation to address the spatial multi-scale needs and a sequential implicit-explicit time splitting infrastructure to address the temporal multi-scale requirements. These approaches are being implemented within the LLNL-developed GEOS HPC computational geosciences framework. We summarize our progress towards realizing such a framework and offer not only a new method to address numerical issues in resolving large shear strains across explicitly resolved interfaces but also how such models as well as topological mesh changes are implemented in the scalable, HPC GEOS framework to represent hydraulic fracture stimulation.

This paper also details preliminary results for applying the initial step in the implementation of this strategy by using a simplified micro-scale model of sub-RVE scale micro seismicity evolution. Though simple, it captures reasonable source mechanisms and is easily extendible to more complicated mechanisms and can be used as a component to a more comprehensive sequential multi-scale approach. This also indicates the likelihood that simple improvements in the constitutive joint model may provide the necessary fidelity to capture a number of other salient features of the source mechanism distribution for microseisms. Finally, by applying a coupled seismo-hydro-mechanical simulation to the problem of two propagating, 3D hydraulic fractures, we have gained useful insight into the hydraulic fracturing process as well as the interpretation of micro seismic data. The suggestion from initial simulations is that rotation of the stress tensor away from the directly fractured zone can initiate seismic responses in areas that are not connected to the propagating hydraulic fractures, which may indicate that micro seismic data yields information on the convolution of damage-induced from propagating hydraulic fractures as well as stress re-orientation within the reservoir.

9. ACKNOWLEDGMENTS

The authors wish to thank Drs. Rob Mellors and Sean Ford at LLNL for their analysis of source mechanisms and Dr. Pengcheng Fu for his analysis of racing hydraulic fractures in an EGS system.

This work was performed under the auspices of the U.S. Department of Energy by Lawrence Livermore National Laboratory under Contract DE-AC52-07NA27344.

REFERENCES

1. Henry, J. T., 1873. *The early and later history of petroleum*. Philadelphia, PA: Jas. B. Rodgers Co.
2. Montgomery, C. T., and M. B. Smith. 2010. *Hydraulic Fracturing: History of an Enduring Technology*. Journal of Petroleum Technology.
3. Newell, R. G. 2011. *The Long-term Outlook for Natural Gas*. Washington, D.C.: Energy Information Administration.
4. Vagnetti, R., and S. McSurdy. 2009. *Modern shale gas development in the United States: a primer*. Ground Water Protection Council report to U.S. Department of Energy. DE-FG26-04NT15455.
5. Moos, D., G. Vassilellis, R. Cade, J. Franquet, A. Lacazette, E. Bourtembourg, and R. Cade. 2011. *Predicting shale reservoir response to stimulation in the upper Devonian of West Virginia*. SPE Annual Technical Conference and Exhibition. SPE-145849.
6. Zoback, M. D., A. Kohli, I. Das, and M. Mcclure. 2012. *The Importance of Slow Slip on Faults During Hydraulic Fracturing Stimulation of Shale Gas Reservoirs*. SPE-155476.
7. Perkins, T. K., and L. R. Kern. 1961. *Widths of hydraulic fractures*. Journal of Petroleum Technology. Sept., p. 937–949.
8. Detournay, E., and D. I. Garagash. 2003. *The near-tip region of a fluid-driven fracture propagating in a permeable elastic solid*. Journal of Fluid Mechanics, 494, p. 1–32.
9. Hakim, V., and A. Karma. 2005. *Crack Path Prediction in Anisotropic Brittle Materials*. Physical Review Letters, 95 (23) 1–4.
10. Hakim, V., and A. Karma. 2008. Laws of crack motion and phase-field models.
11. Pons, A. J., and A. Karma. 2010. *Helical crack-front instability in mixed-mode fracture*. Nature, 464 (7285) 85–9.
12. Wu, H., E. Golovin, Y. Shulkin, A. Chudnovsky, J. W. Dudley, and G. K. Wong. 2008. *Observations of hydraulic fracture initiation and propagation in a brittle polymer*. In *Proceedings of the 42nd U.S. Rock Mechanics Symposium*, San Francisco, CA, 29 June – 2 July, 2008. ARMA 08-321.
13. Warpinski, N. R. 2011. *Fracture Growth in Layered and Discontinuous Media*. Report: Pinnacle, Halliburton.
14. Warpinski, N. R., and L. W. Teufel, 1987. *In situ stresses in low-permeability, nonmarine rocks*. In *Proceedings of the 1987 SPE/DOE Symposium on Low Permeability Reservoirs*. Denver, CO, 18-19 May, 1987. p. 125–138.
15. Casas, L., J. L. Miskimins, A. Black, and S. Green. 2006. *Laboratory hydraulic fracturing test on a rock with artificial discontinuities*. In *Proceedings of the*

SPE Annual Technical Conference and Exhibition. San Antonio, TX. 24-27 September, 2006. SPE-103617.

16. Olson, J., and A. Dahi-taleghani. 1988. *Influence of Natural Fractures on Hydraulic Fracture Propagation*. AAPG Bulletin, 72.
17. Adachi, J., E. Siebrits, A. Peirce, and J. Desroches. 2007. *Computer simulation of hydraulic fractures*. *International Journal of Rock Mechanics and Mining Sciences*. 44, p. 739–757.
18. Odling, N. 1997. *Scaling and connectivity of joint systems in sandstones from western Norway*. *Journal of Structural Geology*. 19 (10) p. 1257–1271.
19. Bonnet, E., O. Bour, N. E. Odling, P. Davy, I. Main, P. Cowie, and B. Berkowitz. 2001. *Scaling of fracture systems in geological media*. *Reviews of Geophysics*. 39 (3) p. 347.
20. Bour, Olivier, and Philippe Davy. 1999. *Clustering and Size Distributions of Fault Patterns: Theory and Measurements*. *Geophysical Research Letters*. 26 (13), p. 2001–2004.
21. Fu, P., S. M. Johnson, and C. Carrigan. 2012. *An explicitly coupled hydro-geomechanical model for simulating hydraulic fracturing in complex discrete fracture networks*. *International Journal for Numerical and Analytical Methods in Geomechanics*.
22. Fu, P., S. M. Johnson, R. R. Settgast, and C. R. Carrigan. 2012. *Generalized displacement correlation method for estimating stress intensity factors*. *Engineering Fracture Mechanics*. 88, p. 90–107.
23. Settgast, R. R., and M. M. Rashid. 2009. *Continuum coupled cohesive zone elements for analysis of fracture in solid bodies*. *Engineering Fracture Mechanics*. 76 (11), p. 1614–1635.
24. Settgast, R. R. 2006. *Numerical modeling of 3-dimensional surface separation*. PhD Thesis, University of California, Davis.
25. Vorobiev, O. 2011. *Simple Common Plane contact algorithm*. *International Journal for Numerical Methods in Engineering*. 90 (2), p. 243-268.
26. Ishida, T., Q. Chen, and Y. Mizuta. 1997. *Effect of Injected Water on Hydraulic Fracturing Deduced from Acoustic Emission Monitoring*. *Pure and Applied Geophysics*. 150 (3), p. 627–646.
27. Matsunaga, I., H. Kobayashi, S. Sasaki, and T. Ishida. 1993. *Studying hydraulic fracturing mechanisms by laboratory experiments with acoustic emission monitoring*. *International Journal of Rock Mechanics and Mining Sciences & Geomechanics Abstracts*. 30 (7), p. 909–912.
28. Julian, B., G. R. Foulger, F. C. Monatero, and S. Bjornstad. 2010. *Imaging hydraulic fractures in a geothermal reservoir*. *Geophysical Research Letters*. 37 (L07305).
29. Barton, N. 1972. *A model study of rock-joint deformation*. *International Journal of Rock Mechanics and Mining Sciences & Geomechanics Abstracts*. 9 (5), p. 579–582.
30. Barton, N., S. Bandis, and K. Bakhtar. 1985. *Strength, deformation and conductivity coupling of rock joints*. *International Journal of Rock Mechanics and Mining Sciences & Geomechanics Abstracts*. 22 (3), p. 121–140.
31. Heuze, F. E., and J. P. Morris. 2006. *Insights into ground shock in jointed rocks and the response of structures there-in*. LLNL Report: UCRL-JRNL-221379.
32. Morris, J.P. 2003. *Review of Rock Joint Models*. LLNL Report: UCRL-ID-153650.
33. Olsson, R., and N. Barton. 2001. *An improved model for hydromechanical coupling during shearing of rock joints*. *International Journal of Rock Mechanics and Mining Sciences*. 38 (3), p. 317–329.
34. Olsson, W. A., and S. R. Brown. 1993. *Hydromechanical Response of a Fracture Undergoing Compression and Shear*. *International Journal of Rock Mechanics and Mining Science & Geomechanics Abstracts*. 30 (7), p. 845–851.
35. Matsuki, K., 2008, Estimation of closure of a fracture under normal stress based on aperture data: International Journal of Rock Mechanics and Mining Sciences, v. 45, no. 2, p. 194–209, doi:10.1016/j.ijrmms.2007.04.009.
36. Matsuki, K., Y. Chida, K. Sakaguchi, and P. W. J. Glover, 2006, Size effect on aperture and permeability of a fracture as estimated in large synthetic fractures: International Journal of Rock Mechanics and Mining Sciences, 43 (5), p. 726–755.
37. Matsuki, K., Y. Kimura, K. Sakaguchi, a. Kizaki, and a. a. Giwelli, 2010, Effect of shear displacement on the hydraulic conductivity of a fracture: International Journal of Rock Mechanics and Mining Sciences, 47 (3), p. 436–449.
38. Ruina, A. 1983. Slip instability and state variable friction laws. *Journal of Geophysical Research*. 88 (10), p. 359–370.
39. Dieterich, J. 1978. *Time-dependent friction and the mechanics of stick-slip*. *Pure and Applied Geophysics*. 116, p. 790–806.
40. Savitski, A., and E. Detournay. 2002. *Propagation of a penny-shaped fluid-driven fracture in an impermeable rock: asymptotic solutions*. *International Journal of Solids and Structures*. 39, p. 6311–6337.
41. Valko, P., and M. J. Economides. 1993. *A Continuum-Damage-Mechanics Model of Hydraulic Fracturing*. *Journal of Petroleum Technology*. 45 (3), p. 198–205.
42. Valko, P., and M. J. Economides. 1994. *Propagation of Hydraulically Induced Fractures a Continuum Damage Mechanics Approach*. *International Journal of Rock Mechanics and Mining Sciences & Geomechanics Abstracts*. 31 (3), p. 221–229.

43. Wu, S., and A. Chudnovsky. 1993. *Effect of microcrack array on stress intensity factor of main crack*. *International Journal of Fracture*. 59, p. 41–52.

44. Shen, X. 2012. *Modeling Fractures with Continuum Damage and Its Numerical Application to Stimulation Estimates*. In *Proceedings of the 46th Rock Mechanics Geomechanics Symposium*. Chicago, IL. ARMA 12–196.

45. Smart, K. J., G. I. Ofoegbu, K. Das, and D. Basu. 2012. *Geomechanical Modeling of Hydraulic Fracture Initiation and Propagation in a Mechanically Stratified Geologic System*. In *Proceedings of the 46th Rock Mechanics Geomechanics Symposium*. Chicago, IL. ARMA 12–275.

46. Swoboda, G., and Q. Yang. 1999. *An energy-based damage model of geomaterials-II. Deduction of damage evolution laws*. *International Journal of Solids and Structures*. 36 (12), p. 1735–1755.

47. Swoboda, G., and Q. Yang. 1999. *An energy-based damage model of geomaterials-I. Formulation and numerical results*. *International Journal of Solids and Structures*. 36 (12), p. 1719–1734.

48. Oda, M. 1984. *Similarity Rules of Crack Geometry in Statistically Homogeneous Rock Masses*. *Mechanics of Materials*. 3, p. 119–129.

49. Cowin, S. C. 1985. *The relationship between the elasticity tensor and the fabric tensor*. *Mechanics of Materials*. 4, p. 137–147.

50. Maleki, K., and A. Pouya. 2010. *Numerical simulation of damage--Permeability relationship in brittle geomaterials*. *Computers and Geotechnics*. 37 (5), p. 619–628.

51. Arson, C., and J.-M. Pereira. 2012. *Influence of damage on pore size distribution and permeability of rocks*. *International Journal for Numerical and Analytical Methods in Geomechanics*. p. DOI: 10.1002/nag.1123.

52. Pereira, J.-M., and C. Arson, 2012, *Retention and Permeability Properties of Damaged Porous Rocks*. *Computers & Geotechnics* (accepted).

53. Suzuki, T. 2012. *Understanding of dynamic earthquake slip behavior using damage as a tensor variable: Microcrack distribution, orientation, and mode and secondary faulting*. *Journal of Geophysical Research*. 117 (B5), p. 1–20.

54. Arson, C., and B. Gatmiri. 2010. *Numerical study of a thermo-hydro-mechanical damage model for unsaturated porous media*. *Annals of Solid and Structural Mechanics*. 1 (2), p. 59–78.

55. Dufour, N., H. Wong, C. Arson, F. Deleruyelle, and J.-M. Pereira. 2012. *A thermodynamically consistent framework for saturated viscoplastic rock-materials subject to damage*. *Mechanics Research Communications*. 45, p. 15–21.

56. Zhao, J. D., D. C. Sheng, and W. Y. Zhou. 2005. *Shear banding analysis of geomaterials by strain gradient enhanced damage model*. *International Journal of Solids and Structures*. 42.

57. Shao, J. F., H. Zhou, and K. T. Chau. 2005. *Coupling between anisotropic damage and permeability variation in brittle rocks*. *International Journal for Numerical and Analytical Methods in Geomechanics*. 29, p. 1231–1247.

58. Mindlin, R. D. 1964. *Micro-structure in linear elasticity*. *Archiv Rational Mech. Anal.* 16, p. 51–78.

59. Vardoulakis, I., and J. Sulem. 1995. *Second-grade plasticity theory for geomaterials*. In *Bifurcation Analysis in Geomechanics*. Blackie Academic and Professional, p. 282–425.

60. Chambon, R., D. Caillerie, and C. Tamagnini. 2001. *A finite deformation second gradient theory of plasticity*. *CR. Acad. Sci. Paris*. T.329, série IIb, p. 797–802.

61. Chambon, R., D. Caillerie, and C. Tamagnini. 2004. *A strain space gradient plasticity theory for finite strain*. *Comput. Methods Appl. Mech. Engrg.*. 193, p. 2797–2828.

62. Matsushima, T., R. Chambon, and D. Caillerie. 2000. *Second gradient models as a particular case of microstructured models: a large strain finite element analysis*. *C.R. Acad. Sci. Paris*. T.328, série IIb, p. 179–186.

63. Tamagnini, C., R. Chambon, and D. Caillerie. 2001. *A second-gradient elastoplastic cohesive-frictional model for geomaterials*. *C.R. Acad. Sci. Paris*. T.329, série IIb, p. 735–739.

64. Frémond, M., and B. Nedjar. 1996. *Damage, Gradient of Damage and Principle of Virtual Power*. *International Journal of Solids and Structures*. 33, p. 1083–1103.

65. Hao, Y., P. Fu, S. Johnson, and C. Carrigan. 2012. *Numerical studies of coupled flow and heat transfer processes in hydraulically fractured geothermal reservoirs*. In *Proceedings of the 36th Annual Geothermal Research Council Meeting*.

66. Hao, Yue, Pengcheng Fu, and C. R. Carrigan. 2013. *Application of a dual-continuum model for simulation of fluid flow and heat transfer in fractured geothermal reservoirs*. In *Proceedings of the 38th Stanford Geothermal Workshop*. Palo Alto, CA.

67. Antoun, T., S. Bohlen, J. Friedmann, P. Fu, R. Settgast, S. Johnson, and S. Ezzedine. 2012. *Advanced computational models of rock fracture mechanics for shale gas development*. In *Proceedings of the Applied Geosciences Conference*.

68. Settgast, R. R., and S. M. Johnson. 2012. *Simulation of hydraulic fracture networks in three dimensions*. In *Proceedings of the Stanford Geothermal Workshop*. Palo Alto, CA.

69. Settgast, R. R., S. M. Johnson, and S. Walsh. 2012. *Hydraulic fracturing: insights from field, lab, and numerical studies*. In *Proceedings of the Fall Meeting*

of the American Geophysical Union. San Francisco, CA.

70. Johnson, S., and J. Morris. 2009. *Caprock Integrity in Carbon Sequestration*. In *Proceedings of the 44th US Rock Mechanics Symposium*.

71. Walsh, S., R. Settgast, and S. Johnson. 2012. *A laboratory and numerical study of chemo-mechanically mediated permeability evolution in the near-wellbore region*. In *Proceedings of the 46th Meeting of the American Rock Mechanics Association*. Chicago, IL.

72. Dieterich, J., K. Richards-dinger, and D. Smith. 2011. *Characteristics of Earthquake Occurrence Fault System Simulations*. Report: UC-Riverside.

73. Dieterich, James H., and K. B. Richards-Dinger. 2010. *Earthquake Recurrence in Simulated Fault Systems*. *Pure and Applied Geophysics*. 167 (8-9), p. 1087–1104.

74. Richards-Dinger, K., and J. H. Dieterich. 2012. *RSQSim Earthquake Simulator*. *Seismological Research Letters*. 83 (6), p. 983–990.

75. Tullis, T. E. et al.. 2012. *A Comparison among Observations and Earthquake Simulator Results for the allcal2 California Fault Model*. *Seismological Research Letters*. 83 (6), p. 994–1006.

76. Zoback, M. D., and S. M. Gorelick. 2012. *Earthquake triggering and large-scale geologic storage of carbon dioxide*. *Proceedings of the National Academy of Sciences of the United States of America*. 109 (26), p. 10164–8.